http://dx.doi.org/10.5935/0103-5053.20140243

J. Braz. Chem. Soc., Vol. 25, No. 12, 2339-2349, 2014.
Printed in Brazil - ©2014 Sociedade Brasileira de Química
0103 - 5053 $6.00+0.00

Article

Cobalt Catalyst Characterization for Methane Decomposition and Carbon Nanotube Growth

Hugo A. Oliveira,[a] Dante F. Franceschini[b] and Fabio B. Passos[*,a]*

[a]*Departamento de Engenharia Química e Petróleo, Universidade Federal Fluminense, Rua Passos da Pátria, 156, 24210-240 Niterói-RJ, Brazil*

[b]*Instituto de Física, Universidade Federal Fluminense, Av. Milton Tavares de Souza, s/n, 24210-341 Niterói-RJ, Brazil*

Varias técnicas, como fisissorção, espectroscopia de fotoelétrons excitados por raios X (XPS), difração de raios X (XRD), redução à temperatura programada (TPR) e quimissorção foram usadas para a caracterização de catalisadores de $Co/\gamma Al_2O_3$ para a produção de nanotubos de carbono por deposição de metano. Os catalisadores apresentaram três principais espécies de cobalto: $CoAl_2O_4$, CoO e Co_3O_4. As espécies de $CoAl_2O_4$ estavam bem dispersas nos catalisadores e apresentaram elevada temperatura de redução, fazendo com que estas espécies sejam inativas para a produção de nanotubos. Para o catalisador $1\%Co/Al_2O_3$, a principal espécie encontrada foi o $CoAl_2O_4$. Contudo, com o aumento do teor de cobalto nos catalisadores, ocorreu um aumento na formação das espécies Co_3O_4 em relação às espécies CoO e $CoAl_2O_4$. Os catalisadores 2 e $3\%Co/Al_2O_3$ apresentaram aglomeração das partículas de cobalto após a etapa de redução e baixa seletividade para produção de nanotubos. Entretanto, o catalisador $4\%Co/Al_2O_3$ não apresentou aglomeração, resultando em uma melhor seletividade para formação de nanotubos, 71%, principalmente do tipo nanotubos de carbono de paredes múltiplas (MWNT).

Several analytical techniques, such as N_2 physisorption, X-ray photoelectron spectroscopy (XPS), X-ray diffraction (XRD), temperature programmed reduction (TPR) and chemisorption were employed to characterize the structure of $Co/\gamma Al_2O_3$ catalysts used for the production of carbon nanotubes by methane vapor deposition. The catalysts were studied after the calcination step and presented three main cobalt species, $CoAl_2O_4$, CoO and Co_3O_4. The $CoAl_2O_4$ species were well dispersed and were reduced only at high temperatures, rendering them inactive for the carbon nanotube production. In the case of the $1\%Co/Al_2O_3$ catalyst, the main cobalt species found was $CoAl_2O_4$. However, increasing the cobalt content in the catalysts led to a higher formation of Co_3O_4 as compared to CoO and $CoAl_2O_4$ species. The 2 and $3\%Co/Al_2O_3$ catalysts showed particle agglomeration during the pretreatment step that decreased selectivity towards nanotube production. The $4\%Co/Al_2O_3$ catalyst did not show particle agglomeration and presented a higher selectivity to carbon nanotube production, 71%, mainly multi-walled carbon nanotubes (MWNT).

Keywords: carbon nanotubes, cobalt, catalyst support, chemical vapor deposition, methane

Introduction

Carbon nanotubes (CNT) exhibit unique physical and chemical properties that have opened a vast number of applications and new ones are still under development. However, for the incorporation of CNT into everyday materials, it is important to control their growth. The production of CNT with pre-determined specifications is an essential requirement for their industrial use. The investigation into CNT production by catalytic chemical vapor deposition (CVD) has attracted great attention and has become the most popular synthesis method due to its easy setup and scale-up for mass production.[1,2]

Many researchers[3-5] have studied different catalyst formulations and operating conditions for CVD process improvement. Cobalt-supported catalysts have shown high selectivity towards CNT production. The nature and morphology of the cobalt species affects the catalyst activity and selectivity on CNT production. So, it is important to understand the influence of these cobalt species on carbon

*e-mail: fbpassos@vm.uff.br

nanotube production in order to develop a strategy to maximize the catalyst selectivity and activity. In our previews work,[6] among various catalyst formulations investigated, cobalt catalysts supported on alumina exhibited the highest carbon nanotube yield. Therefore, this contribution has focused on the characterization of the cobalt species present in a cobalt/alumina system for each step of CNT growth and explored their influence in CNT synthesis.

In our CNT production method, there are two main steps: reduction of the oxide catalyst followed by methane decomposition on the reduced catalyst for carbon nanotube growth. Therefore, 1, 2, 3 and 4 wt.% Co/Al_2O_3 catalysts were studied in three different states, as an oxide, reduced and passivated.

The catalysts were investigated using energy-dispersive X-ray spectroscopy (EDX), X-ray diffraction (XRD), N_2 physisorption, temperature programmed reduction (TPR), CO and H_2 chemisorption and X-ray photoelectron spectroscopy (XPS). The combination of these techniques can detail the structure of the catalysts, which can be used to clarify the activity and selectivity toward carbon nanotube formation.

CNT characterization was performed by Raman spectroscopy, temperature programmed oxidation (TPO), scanning electron microscopy (SEM) and transmission electron microscopy (TEM).

Experimental

Catalyst preparation

The Al_2O_3 support was obtained by drying bohemite (Catapal-A, Sasol, degree of purity: 99.9%) in air at 120 °C for 16 h and then calcining in air at a heating rate of 10 °C min^{-1} up to 550 °C for 2 h. A series of 1, 2, 3 and 4 wt.% Co/Al_2O_3 catalysts was prepared by incipient wetness impregnation using a solution of $Co(NO_3)_2.6H_2O$ (Merck, degree of purity: 99.8%). After impregnation, the catalysts were dried in air at 120 °C for 16 h and then calcined in air for 2 h at 550 °C.

Catalyst characterization

The oxide catalysts were studied after the calcination step. For the reduced state, the oxide catalysts were reduced under H_2 flow from room temperature to 700 °C at a heating rate of 10 °C min^{-1} and were then analyzed. For the passivated state, the samples were reduced as described above and then the catalysts were cooled to room temperature in He flow. Finally, they were passivated with 1.0% O_2/He (30 mL min^{-1}) during 2 h at room temperature.

Measurements of surface area, pore volume and pore diameter distribution were performed in a Micromeritics ASAP 2010 apparatus by N_2 adsorption. The oxide catalysts were evacuated at 220 °C during 4 h before analysis. Pore volume and pore diameter distribution were calculated from the N_2 desorption curve using the Barrett-Joyner-Halenda (BJH) method.

The chemical compositions of the oxide catalysts were determined by EDX in vacuum using an EDX-720 Shimadzu apparatus.

XPS experiments of the oxide and passivated catalysts were performed with a Thermo Scientific ESCALAB 250Xi with monochromatic Al Kα X-rays with a spot size of 650 μm. The base pressure inside the analysis chamber was 1×10^{-9} mbar or lower. The samples were mounted on a sample holder by means of a double-sided adhesive carbon tape. For the survey spectra an energy step size of 1.0 eV and a pass energy of 100 eV were used. For the individual element spectra, Co2p, O1s and Al2p, an energy step size of 0.05 eV and a pass energy of 25.0 eV were used. The flood gun was used to neutralize charge buildup on the surface of the samples. The spectra were analyzed and peak fitted with a linear type background and a Gaussian product function.

XRD experiments of the oxide and passivated catalysts were performed in a Rigaku Miniflex diffractometer with monochromatic Cu Kα (1.540 Å) radiation with a scan rate of 0.05° min^{-1} in the range of $2\theta = 2.00$ to 80.00°. The average cobalt particle sizes were calculated from the most intense Co_3O_4 line, $2\theta = 36.9°$, using the Scherrer formula.

Raman spectroscopy was used for the characterization of the oxide catalysts and carbon deposits on the catalysts after the reaction step. Raman spectra were taken in a Confocal Raman Microscope alpha 300, Witec, using a 50× objective lens and green laser with 532 nm wavelength. The integration time was 1.0 s and the number of scans was 500.

TPR experiments were performed in a U-shaped tubular quartz reactor coupled to a quadrupole mass spectrometer (Omnistar, Balzers). The oxide catalysts, approximately 0.5 g, were dried in He for 30 min at 150 °C before TPR. After cooling to room temperature, a mixture of 5% H_2/Ar flowed (30 mL min^{-1}) through the catalyst and the temperature was raised at a heating rate of 10 °C min^{-1} up to 1000 °C.

H_2 and CO chemisorptions were performed using a volumetric method in a Micromeritcs ASAP 2010 device. The pretreatment of the oxide catalysts consisted of drying at 220 °C for 30 min under a 30 mL min^{-1} He flow before the reduction. After cooling to room temperature, the reduction step was performed. The temperature was raised at a heating rate of 10 °C min^{-1} up to 700 °C under 30 mL min^{-1} of H_2. Then, the reduced catalysts were outgassed under

vacuum at 700 °C before cooling to 150 °C, where the H_2 chemisorption measurements were performed. Then, the catalysts were evacuated at 500 °C, and finally the CO chemisorption measurements were done at 35 °C. H_2 and CO chemisorption on cobalt are performed at temperatures higher than room temperature as they are activated.[7] Total and reversible isotherms were measured at the pressure range of 10-300 mmHg. The amount of H_2 and CO adsorbed in each measurement was determined by extrapolating the linear part of the isotherm to zero pressure. It is assumed that the adsorption stoichiometries for H_2 and CO are H/Co = 1 and CO/Co = 1, respectively. The Co particle size was calculated supposing spherical Co particles. For H_2 chemisorption, these calculations were performed assuming total chemisorption as recommended by Reuel and Bartholomew.[8]

CNT production

For the CNT production by methane CVD, 1.0 g of catalyst was inserted into a quartz boat and then placed in a horizontal tubular quartz reactor. The catalyst was heated under 200 mL min^{-1} H_2 flow from room temperature to 700 °C at a heating rate of 10 °C min^{-1}. Then, the H_2 flow was switched to 200 mL min^{-1} methane for 30 min. Finally, the sample was cooled to room temperature under Ar flow.

CNT characterization

TPO experiments were performed in the same apparatus described for the TPR experiments. The samples (0.2 g) were dried in He for 30 min at 200 °C before TPO. Afterwards, the sample was cooled to room temperature, a 5% O_2/He mixture flowed through the sample at 30 mL min^{-1} as the temperature was raised at a heating rate of 10 °C min^{-1} up to 1000 °C. There was always O_2 in excess to avoid the formation of carbon monoxide. The mass of carbon present in each sample was determined by the evolution of CO_2.

CNT morphology was analyzed by SEM images. SEM images were performed in a Zeiss EVO MA and a Jeol JSM-5800 LV scanning electron microscopes with electron beam energy in the 10-30 kV range.

The TEM images were obtained in a FEI Tecnai F30 transmission electron microscope. For this experiment, the samples were dispersed in isopropanol and ultrasonicated for 15 min. Then, a few drops of the resulting suspension were deposited on a grid and subsequently evaporated.

Results and Discussion

N_2 physisorption

N_2 physisorption measurements were performed to determine the changes in surface area and pore diameter distribution between the support and catalyst after the calcination step. Table 1 shows the textural properties of the support and cobalt catalysts. The surface area and the average pore diameter of the alumina are typical of γ-phase, as found by Rane *et al.*.[9]

Higher cobalt loading catalyst showed lower surface area and pore volume. This may be attributed to the blocking of narrow pores by the cobalt oxide particles. Since the narrow pores are blocked, there is an increase in average pore diameter as shown in Figure 1 and Table 1.

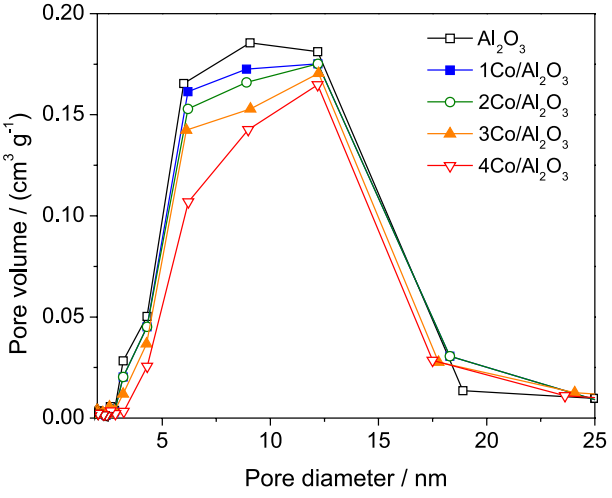

Figure 1. Support and catalyst pore size distribution.

Table 1. Textural properties and chemical composition of the catalysts

Sample	Surface area / (m^2 g^{-1})	Pore volume / (cm^3 g^{-1})	Average pore diameter / nm	Bulk Co[a] / wt.%	Surface Co[b] / wt.%	Fraction of Co as $CoAl_2O_4$ [b]
Al_2O_3	282	0.64	7.1	–	–	–
$1Co/Al_2O_3$	266	0.63	7.4	0.92	1.10	0.93
$2Co/Al_2O_3$	257	0.61	7.5	2.02	0.54	0.82
$3Co/Al_2O_3$	256	0.61	7.5	2.99	0.56	0.69
$4Co/Al_2O_3$	248	0.59	7.8	3.96	0.74	0.52

[a]Measured by EDX; [b]measured by XPS.

Energy-dispersive X-ray spectroscopy

The catalyst chemical composition was analyzed by EDX. The cobalt fraction is consistent with the nominal value used in the catalyst preparation. Table 1 shows the cobalt composition of the catalysts.

X-ray photoelectron spectroscopy

XPS can be used to determine the surface chemical composition of the catalyst. Two survey spectra were obtained at different points for each catalyst and they showed the same profile. This indicates a uniform cobalt distribution on the support. The survey spectrum detected four elements: cobalt, aluminum, oxygen and carbon. The carbon comes from adventitious hydrocarbons nearly always present on samples, introduced from the laboratory environment or from adhesive carbon tape.

The cobalt composition found by XPS is a function of its depth and surface distribution. So, when cobalt particles are concentrated in the top layers of the catalyst or they are highly dispersed on the support, the intensity of the cobalt X-ray photoelectron is increased. $1Co/Al_2O_3$ showed approximately the same surface cobalt concentration as its bulk value, Table 1. This is an indicative that the cobalt particles are uniformly distributed within the catalyst pellet.

Usually, three different cobalt species are present in a Co/Al_2O_3 catalyst: Co_3O_4, CoO and $CoAl_2O_4$. Each of these cobalt species shows a different color; cobalt aluminate is light blue, CoO is olive greenish-brown and Co_3O_4 is black.[10,11] $1Co/Al_2O_3$ catalysts presented a light blue color, indicating that most of the cobalt is in the form of cobalt aluminate. Increasing the cobalt loading of the catalysts, they became darker until turning black for $4\%Co/Al_2O_3$. So, the amount of Co_3O_4 species increased with cobalt loading and XPS helped in identifying these species.

The identification of cobalt chemical states depends on the accurate determination of the binding energy lines. The flood gun technique was used to neutralize charge build-up on the sample surface. However, the flood gun may provide more electrons to the catalyst than those leaving it. As a result, the whole catalyst surface may charge up due to the energy of the flood gun beam. For this reason, the peak energies were corrected by reference to the C1s line at 284.8 eV. In our experiments, there was an excessive charge compensation making the peaks shift to lower binding energy at values of 0.5, 0.4, 0.3 and 0.2 eV for the catalysts with cobalt loadings of 1, 2, 3 and 4 wt.%, respectively. Other authors, such as Hilmen *et al.*,[12] have corrected the peak energy by reference to Al2p. In our results, there was no significant difference between the correction by reference to the C1s line or to the Al2p line.

The binding energy of the cobalt species present on the catalysts can be compared to the binding energy of reference compounds, such as Co_3O_4, CoO and $CoAl_2O_4$.[3,12,13] According to Hilmen *et al.*,[12] the binding energy of the $Co2p_{3/2}$ peak is found at 780.2 eV for a Co_3O_4 bulk sample and its asymmetric shape can be explained due the slightly higher binding energy of Co^{2+} in relation to Co^{3+} (780.3 and 779.5 eV, respectively). For a bulk CoO sample, Herrera *et al.*[3] found a binding energy of 780.5 eV for the $Co2p_{3/2}$ peak. As these cobalt species show approximately the same binding energy, it is hard to distinguish these peaks precisely. However, the $Co2p_{3/2}$ peak of $CoAl_2O_4$ is found at higher binding energy, 782.0 eV, than the binding energy of the $2p_{3/2}$ peak of Co_3O_4 and CoO. In this way, it is possible to distinguish the cobalt aluminate $Co2p_{3/2}$ peak from the other cobalt species. Therefore, the amount of $CoAl_2O_4$ could be estimated by deconvolution of the $Co2p_{3/2}$ peak into two mixed Gaussian-Lorentzian curves centered at a fixed binding energy peak, 780 eV for CoO and Co_3O_4 species and 782.0 eV for $CoAl_2O_4$. Figure 2 shows the XPS spectra of the oxide catalyst for the Co2p region and Table 1 shows the fraction of cobalt aluminate present on the catalysts.

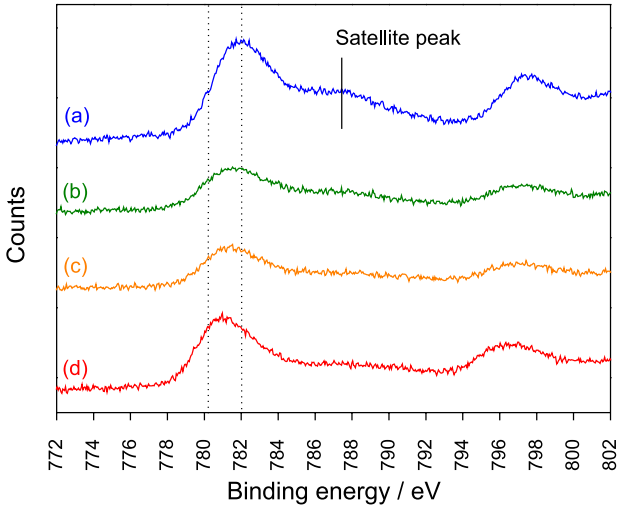

Figure 2. XPS spectra of the oxide catalyst in the Co2p region. (a) $1Co/Al_2O_3$; (b) $2Co/Al_2O_3$; (c) $3Co/Al_2O_3$; (d) $4Co/Al_2O_3$. The vertical dot lines are binding energy reference compounds: Co_3O_4 (780.2 eV) and $CoAl_2O_4$ (782.0 eV).[12]

The $Co2p_{3/2}$ peak of the $1Co/Al_2O_3$ catalyst has the same binding energy of the $CoAl_2O_4$ bulk sample, as found by Hilmen *et al.*.[12] It shows that most of the cobalt species on the $1Co/Al_2O_3$ catalyst is $CoAl_2O_4$. Increasing the cobalt content on the catalysts, the binding energy of the $Co2p_{3/2}$ peak shifted to lower energy and the satellite peak intensity decreased. The first effect shows an increase of the CoO

and Co_3O_4 fraction in relation to $CoAl_2O_4$ and the second effect points to an increase of Co_3O_4 species in relation to CoO. The satellite peak intensity is weaker for Co_3O_4 than for CoO and centered about 10 eV from the main peaks.[13] In our results, the satellite peak could only be observed in the case of the $1Co/Al_2O_3$ catalyst, Figure 2.

The Co_3O_4 and $CoAl_2O_4$ species represent the two limit cases of cobalt/alumina interaction in a catalyst. The Co_3O_4 species has no any interaction with alumina while $CoAl_2O_4$ shows complete spinel formation.[12]

Kerkhof and Moulijn[14] have shown that the supported phase/support signal intensity ratio is related to the dispersion of the supported phase. In this model, the catalyst is supposed to consist of several sheets of the support with cubic particles of equal size in between. Thus, the oxide cobalt particle size can be estimated from the $Co2p_{3/2}$ and Al2p intensity ratio, $(I_{Co}/I_{Al})_{crystallite}$, according to equation 1:

$$\frac{\left(\frac{I_{Co}}{I_{Al}}\right)_{crystallite}}{\left(\frac{I_{Co}}{I_{Al}}\right)_{monolayer}} = \frac{1-e^{a}}{\alpha} \quad (1)$$

where $\alpha = \frac{C}{\lambda_{Co}}$, c is the cube edge length of the average cobalt particle and λ_{Co} is the mean escape depth of the photoelectrons from cobalt passing through cobalt oxide.

The predicted monolayer intensity of Co and Al were calculated using the Kerkhof and Moulijn model,[14] according to equation 2:

$$\left(\frac{I_{Co}}{I_{Al}}\right)_{monolayer} = \left(\frac{n_{Co}}{n_{Al}}\right)_{bulk} \frac{D(\varepsilon)_p}{D(\varepsilon)_s}\left(\frac{\sigma_{Co}}{\sigma_{Al}}\right)\frac{\beta_1(1+e^{-\beta_2})}{2(1-e^{-\beta_2})} \quad (2)$$

where $\beta_1 = t / \lambda_{(Al/Al)}$ and $\beta_2 = t / \lambda_{(Co/Al)}$. $\lambda_{(Al/Al)}$ is the mean escape depth of the photoelectrons from aluminum passing through the alumina, λ_{CoAl} is the mean escape depth of the photoelectrons from cobalt passing through the alumina and t is mean thickness of the alumina. The term $(n_{Co}/n_{Al})_{bulk}$ is the bulk atomic ratio of cobalt and aluminum from the catalysts. The mean escape depth of the photoelectrons used were obtained from Penn.[15]

The detector efficiency D is a function of the kinetic energy of the electrons and σ is the photoelectron cross sections. These parameters were substituted by the atomic sensitivity factor from the Avantage Software library, 12.62 for $Co2p_{3/2}$ and 0.537 for Al2p.

For the $1Co/Al_2O_3$ catalyst, the ratio between the measured $Co2p_{3/2}$ and Al2p intensity ratios and the predicted monolayer intensity ratio is 1.28 as shown in Table 2. As this ratio cannot be higher than 1, this result indicates that cobalt aluminate is not dispersed as in the Kerkhof and Moulijn model. For the other catalysts, the average $CoAl_2O_4$ particle size was estimated. The cobalt aluminate particle size increased with the cobalt content. As the cobalt $Co2p_{3/2}$ peak from CoO and Co_3O_4 have approximately the same binding energy, it was not possible to separate these peaks precisely. Hence, the average particle size of CoO and Co_3O_4 were estimated together. The average cobalt oxide size also increased with cobalt content and they are larger than the $CoAl_2O_4$ particles. The cobalt particle size is shown in Table 2.

For the $1CoAl_2O_3$ catalyst, a highly dispersed cobalt aluminate may be formed by cobalt atom migration into the bulk alumina matrix, as found by Liotta *et al.*[16] and Jongsomjit *et al.*.[17]

The $1Co/Al_2O_3$ catalyst presented only $CoAl_2O_4$ species as found by XPS, a surface analysis, and by TPR, a bulk analysis (see TPR section, below). This catalyst showed approximately the same $CoAl_2O_4$ concentration on the surface (XPS measurements) and in the bulk phase, as found by EDX analysis (Table 1). Application of the Kerkhof and Moulijn model has also shown that the cobalt aluminate species remain highly dispersed in the other catalysts as in the case of $1Co/Al_2O_3$. In this way, the $CoAl_2O_4$ concentration on the surface was assumed as equal to the bulk concentration for all studied catalysts and the total amount of cobalt as $CoAl_2O_4$ present in the catalysts was determined by multiplying the fraction of Co as $CoAl_2O_4$ estimated by XPS by the weight fraction of bulk Co measured by EDX.

Table 2. Average cobalt particle size estimated by XPS intensities, Co_3O_4 crystallite average size calculated by XRD

Sample	$(I_{Co}/I_{Al})_{cryst.} / (I_{Co}/I_{Al})_{mono}$	$CoAl_2O_4$ particle size[a] / nm	Cobalt oxide particle size[a] / nm	Co_3O_4 crystallite size[b] / nm	Fraction of metallic phase[a]
$1Co/Al_2O_3$	1.28	–	–	–	0
$2Co/Al_2O_3$	0.29	2.4	2.4	–	1.5
$3Co/Al_2O_3$	0.20	3.0	4.1	10.0	2.4
$4Co/Al_2O_3$	0.20	3.2	4.3	14.3	8.3

[a]Measured by XPS; [b]measured by XRD.

Increasing the cobalt content in the catalysts, there was an increase in the total amount of $CoAl_2O_4$ up to 2.1 wt.% on the $3Co/Al_2O_3$ catalyst. This shows that there is a maximum limit between 2 and 3 wt.% Co for the $CoAl_2O_4$ formation on the cobalt/alumina catalyst, when it is prepared as in the synthesis conditions described in the experimental section.

X-Ray diffraction

XRD analysis was used to determine the crystalline phases and to estimate the cobalt oxide crystallite size. Figure 3 shows the XRD patterns of the support and oxide catalysts. The diffraction peak at 40.0 and 66.7° are those of γ-Al_2O_3 and they can be observed in all samples.

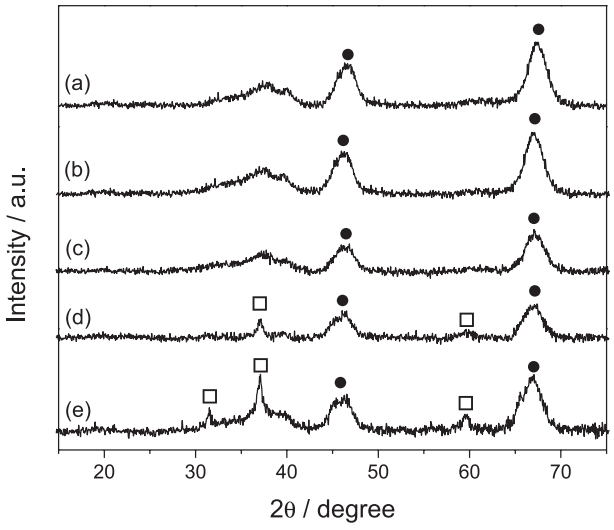

Figure 3. XRD patterns of oxide catalysts: (a) Al_2O_3; (b) $1Co/Al_2O_3$; (c) $2Co/Al_2O_3$; (d) $3Co/Al_2O_3$; and (e) $4Co/Al_2O_3$. □ Co_3O_4 phase; ● γ-Al_2O_3 phase.

The 3 and $4Co/Al_2O_3$ catalysts showed diffraction peaks at 31.3, 36.9 and 59.5°. These diffraction lines can be related to Co_3O_4 or $CoAl_2O_4$ species.[17] In this way, it was not possible to distinguish these two phases by XRD. However, $CoAl_2O_4$ species are well dispersed and there is a maximum on its formation (2.1 wt.%) in the $3Co/Al_2O_3$ catalysts, as found by XPS. This way, the increase in the cobalt diffraction peak intensity from 3 to $4Co/Al_2O_3$ catalysts on the XRD patterns may be attributed to the Co_3O_4 species. The diffraction peaks of CoO, 42.6 and 61.8°,[17] could not be observed in the XRD patterns. It may due to its low loading, which can lead to a very small particle size or the CoO particles were amorphous.

The average Co_3O_4 crystallite size was calculated from the most intense Co_3O_4 peaks at 36.9° using the Scherrer equation. These results can be observed in Table 2.

The average crystallite sizes found by XRD were quite larger than the particle size found by XPS. In the case of XPS, the particle size was estimated from the $Co2p_{3/2}$ peak associated with photoelectrons leaving the CoO and Co_3O_4 particles, not only from the crystalline Co_3O_4 particles. Thus, the particle size calculated by XPS is probably an average of small CoO and large Co_3O_4 particles.

Temperature programmed reduction

TPR can help with the identification and quantification of the cobalt oxide species supported on alumina. The TPR profile for $1Co/Al_2O_3$ didn't show any significant hydrogen consumption, Figure 4a. This shows that there was only irreducible cobalt species present on this catalyst, in the form of $CoAl_2O_4$, as suggested by Jongsomjit *et al.*.[17] XPS analysis showed that 93 wt.% of these species are cobalt aluminate. The presence of this species on the catalysts is not desired, since only metallic cobalt particles are able to decompose methane and grow carbon nanotubes.

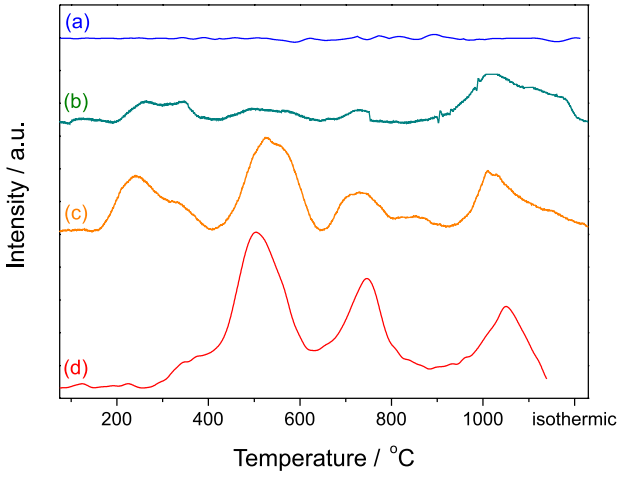

Figure 4. TPR profiles of catalysts (a) $1Co/Al_2O_3$; (b) $2Co/Al_2O_3$; (c) $3Co/Al_2O_3$; and (d) $4Co/Al_2O_3$. The reduction was conducted under 5% H_2/Ar, using a heating rate of 10 °C min^{-1}.

The TPR profile of the $2Co/Al_2O_3$ catalyst showed four small reductions peaks, suggesting that there are four different reducible cobalt species. The peak at 364 °C is attributed to the reduction of an amorphous cobalt oxide similar to bulk Co_3O_4.[18] The peak around 507 °C is attributed to the two-step reduction of Co_3O_4. This reduction temperature is higher than the reduction temperature of a bulk Co_3O_4 sample. This shift to higher temperatures demonstrates that there is an interaction between the support and the cobalt oxide particles.[19] The small peak at 737 °C is associated with the reduction of CoO linked to alumina[19] and the reduction peak at 1000 °C is attributed to reduction of cobalt aluminate.[20]

The irreducible cobalt aluminate present in the $1Co/Al_2O_3$ catalyst may have different structure from the reducible aluminate present in the $2Co/Al_2O_3$ catalyst. The cobalt aluminate spinel may be a partly inverse spinel, in which some Co^{2+} ions are placed in unstable octahedral positions, or a normal spinel, with Co^{2+} ions placed in stable tetrahedral positions. Because of their different stability, Co^{2+} ions in partly inverse spinel are reduced at lower temperatures than in normal spinel.

The reduction profile for the $3Co/Al_2O_3$ catalyst also showed four different reducible cobalt species, as in $2Co/Al_2O_3$. However, the fraction of each reduced cobalt species was different. The fraction of Co_3O_4 (peak at 507 °C) was higher for $3Co/Al_2O_3$ than for $2Co/Al_2O_3$. This peak was also intense in the TPR profile of the $4Co/Al_2O_3$ catalyst, in agreement with its X-ray diffractogram.

The degree of reduction is an important parameter on catalyst activity and different cobalt oxide species require different amounts of hydrogen to be reduced to its metallic form. The fraction of the cobalt present as Co_3O_4 species can be estimated from the hydrogen consumption from 130 to 645 °C. This reduction corresponds to the following reaction: $Co_3O_4 + 4H_2 \rightarrow 3Co + 4H_2O$. Thus, a molar ratio of 1.33 H_2/Co is required. The CoO and $CoAl_2O_4$ species demand a molar ratio of 1H_2/Co for their reduction.[18,19] In this way, it was possible to estimate the total hydrogen consumption for a complete catalyst reduction and the degree of reduction was then calculated. Table 3 shows the degree of reduction for the several catalysts.

The degree of reduction increased with the cobalt content in the catalyst. However, there was a large cobalt fraction that was not reduced in all studied catalysts. The strong interaction between cobalt and alumina can form surface and bulk spinels that are not easily reduced.[21] The trend of increasing degree of reduction with the cobalt content was previously observed for the Co/Al_2O_3 catalysts.[21]

While all Co_3O_4 was reduced to its metallic form, only a small fraction of CoO and $CoAl_2O_4$ was reduced from 645 to 1000 °C. In this way, the overall fraction of CoO and $CoAl_2O_4$ could not be determined by TPR. However, the fraction of CoO can be calculated by the subtraction of the Co_3O_4 fraction determined by TPR from the $CoAl_2O_4$ fraction estimated by XPS. XPS was used to estimate the $CoAl_2O_4$ concentration, considering that this species is uniformly distributed through the catalyst, as discussed before. Figure 5 shows the distribution of cobalt species for the catalysts.

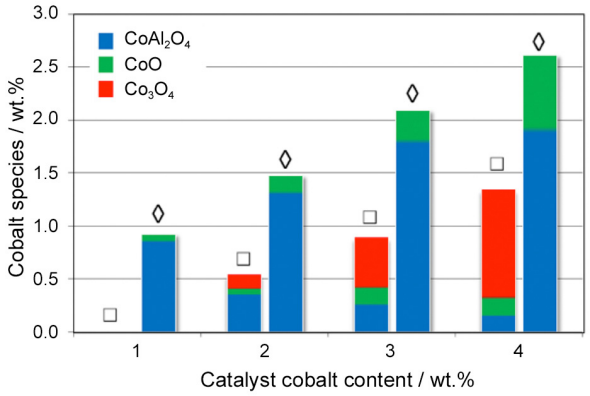

Figure 5. Cobalt species distribution for the catalysts. □ Species that were reduced; ◊ species that were not reducible during TPR experiments.

The increase of cobalt loading on the catalysts led to a higher formation of reducible Co_3O_4 as compared to reducible CoO and $CoAl_2O_4$ species. From Figure 5 we can also note that the weight percentage of cobalt as irreducible $CoAl_2O_4$ did not increase much, increasing with the cobalt content up to the $3Co/Al_2O_3$ catalyst while the formation of irreducible CoO keeps increasing. These changes in composition affect the catalyst color and they became darker with the increase of Co_3O_4 species.

Chemisorption

A better representation of the cobalt particle as it stands before the carbon nanotube reaction can be done by its characterization in the reduced or in the passivated state. The chemisorption measurements may be used to estimate the average metallic particle size. For this, it is necessary to know the catalyst degree of reduction at the beginning of reaction. So, the pretreatment degree of

Table 3. Results from TPR. Oxide catalyst degree of reduction, distribution of cobalt species and degree of reduction of the reduced catalysts (after pretreatment reduction step)

Sample	Degree of reduction / %	Fraction of Co_3O_4	Fraction of CoO and $CoAl_2O_4$	Pretreatment degree of reduction / %
$1Co/Al_2O_3$	0	0	1	0
$2Co/Al_2O_3$	27	0.07	0.93	17
$3Co/Al_2O_3$	30	0.16	0.84	20
$4Co/Al_2O_3$	31	0.24	0.76	22

Table 4. Total and irreversible H_2 and CO chemisorption, dispersion and particle sizes of catalysts obtained from chemisorption

Sample	H_2 / (μmol g^{-1} cat)		CO / (μmol g^{-1} cat)		Total H/Co	Irrever. CO/Co	Particle size / nm	
	Total	Irrever.	Total	Irrever.			Total H_2	Irrever. CO
$1Co/Al_2O_3$	0.0	0.0	0.7	0.0	–	–	–	–
$2Co/Al_2O_3$	2.6	1.1	13.7	10.5	0.010	0.031	12.2	5.5
$3Co/Al_2O_3$	4.5	1.9	25.8	20.7	0.018	0.041	11.2	4.9
$4Co/Al_2O_3$	7.2	3.1	44.6	30.6	0.021	0.046	9.8	4.6

reduction was determined by a new TPR after the reduction step. The difference between the hydrogen consumption for reduction of the oxide catalysts and for the partially reduced catalysts is related to the hydrogen consumption during the reduction pretreatment step. Table 3 shows values of the pretreatment degree of reduction of the catalysts. The pretreatment degree of reduction increased with cobalt loadings up to 22%. After pretreatment, the catalysts show values of degree of reduction similar to the degree of reduction observed after the standard TPR. So, an increase in the temperature of catalyst reduction during the pretreatment reduction step would not increase the final degree of reduction. Additionally, static H_2 and CO chemisorption measurements were used to determine the dispersion and average particle size of the metallic cobalt particles. These reduced species are related to the catalyst activity and structure of carbon nanotube growth. There is a correlation between the size of the catalyst particles and the CNT diameter.[22-24] The average particle size was calculated from total H_2 uptake and from irreversible CO uptake using a stoichiometric adsorption ratio of 2 and 1, respectively. Table 4 shows the total and irreversible H_2 and CO uptakes and average particle size.

H_2 and CO uptakes increased with cobalt loading and higher values were obtained for CO uptake, as previously reported by Reuel and Bartholomew.[8] Besides, the total H/Co and irreversible CO/Co ratios have shown some increase with increasing metal loading. In this way, the $4Co/Al_2O_3$ catalyst showed better metallic dispersion and smaller metallic particle size than 2 and 3 wt.% cobalt catalysts. However, in the oxidized state, the particle size increased with the increase of cobalt loading. Nevertheless, the 2 and 3 wt.% cobalt catalysts showed cobalt oxide particles that are reduced at low temperature (see TPR profile). These metallic particles may have agglomerated on the reduction pretreatment step.

To clarify the cobalt agglomeration during the reduction pretreatment, the reduced catalysts were re-oxidized with 1.0% O_2/He (30 mL min^{-1}) during 2 h at 550 °C. Then, these catalysts were analyzed by XRD. The particle size of the 1 and 2 wt.% cobalt catalysts could not be estimated due the low Co_3O_4 peak signal. However, the particle size of $3Co/Al_2O_3$ increased from 10.0 to 14.3 nm and the $4Co/Al_2O_3$ catalyst didn't change much its particle size, 14.2 nm. These results support the particle agglomeration suggestion during the reduction pretreatment.

These re-oxidized samples were also studied by XPS measurements, Figure 6. There was no significant difference between the XPS spectra of $1Co/Al_2O_3$ in the oxide and passivated state. This result agrees with TPR findings, where no reduction was observed for the $1Co/Al_2O_3$ oxide catalyst. Thus, there was no chemical change in its composition after the reduction and passivation steps. The XP spectrum of the other passivated catalysts showed small differences in their profile in relation to oxide profile. These differences can be observed in the inset graph of Figure 6. The 2, 3 and $4Co/Al_2O_3$ catalysts showed two main peaks in the inset. The first peak, at 778.2 eV, represents the increase of the metallic phase,[3,12] and the second peak (negative), at 780.3 eV, represents the decrease of cobalt as oxide species in the passivated catalyst in relation to the oxide catalysts.

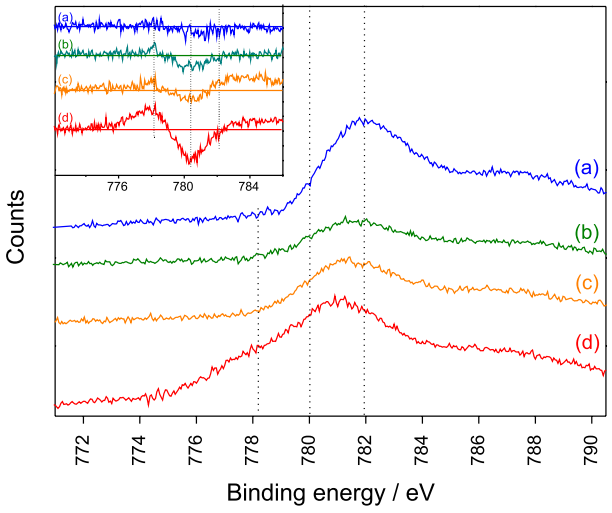

Figure 6. XPS spectra of the passivated catalysts in the Co2p region. The oxide catalysts were reduced in H_2 at 700 °C and then exposed to 1% O_2/He for 2 h at room temperature. (a) $1Co/Al_2O_3$; (b) $2Co/Al_2O_3$; (c) $3Co/Al_2O_3$; and (d) $4Co/Al_2O_3$. The vertical dot lines are binding energy reference compounds: Co^0 (778.2 eV), Co_3O_4 (780.2 eV) and $CoAl_2O_4$ (782.0 eV).[12] Inset: difference on the XPS profile of the oxide and passivated catalysts.

The fraction of metallic phase, R, can also be obtained by using the following equation:[25]

$$R = \frac{1 - \left(\frac{I_{Co}}{I_{Al}}\right)_{crystallite}}{\left(\frac{I_{Co}}{I_{Al}}\right)_{monolayer}} \quad (3)$$

The fraction of metallic phase increased with the cobalt loading, Table 2**.** However, the degree of reduction found by XPS is significantly lower than that calculated by TPR. The passivation step produces a cobalt oxide shell on the metallic cobalt particle and the cobalt fraction on the oxide shell is higher on small particles. Moreover, XPS is a surface method while TPR is a bulk method.

Carbon nanotube production and characterization

TEM

Carbon nanotube production was characterized by SEM and TEM. The SEM images showed low-density carbon deposits in the case of the 1, 2 and 3Co/Al_2O_3 catalysts. However, the 4Co/Al_2O_3 catalyst showed a high carbon density, Figure 7a. Increasing the SEM magnification, the image shows that most of the surface is covered by carbon filaments, Figure 7b. From Figure 7c along with other images, the filament average diameter was estimated as 13 nm (73 filaments measured). The average diameter of metallic cobalt particles found by H_2 chemisorption was approximately the same of the average diameter of the filaments, 14.2 nm. TEM images show that theses filaments are carbon nanotubes and most of them are multi-walled carbon nanotubes (MWNT). Figure 7d shows MWNT growth on the 4Co/Al_2O_3 catalyst.

TPO

The total carbon yield during the reaction step was defined as the mass of carbon deposited *per* mass of catalyst. 1Co/Al_2O_3 didn't show any significant carbon deposition. In this catalyst, most of the cobalt is present as cobalt aluminate and it could not be reduced during the reduction pretreatment. Table 5 shows the total carbon yield for the several catalysts. The carbon yield is proportional to

Table 5. TPO and Raman spectroscopy data of carbon deposits on the catalysts

Carbon deposit on catalyst	Yield / %	Selectivity / %			D/G ratio
		Amorphous	SWNT	MWNT	
1Co/Al_2O_3	0	–	–	–	
2Co/Al_2O_3	12.2	85	11	4	1.3
3Co/Al_2O_3	15.1	80	11	10	1.0
4Co/Al_2O_3	34.1	29	29	42	0.7

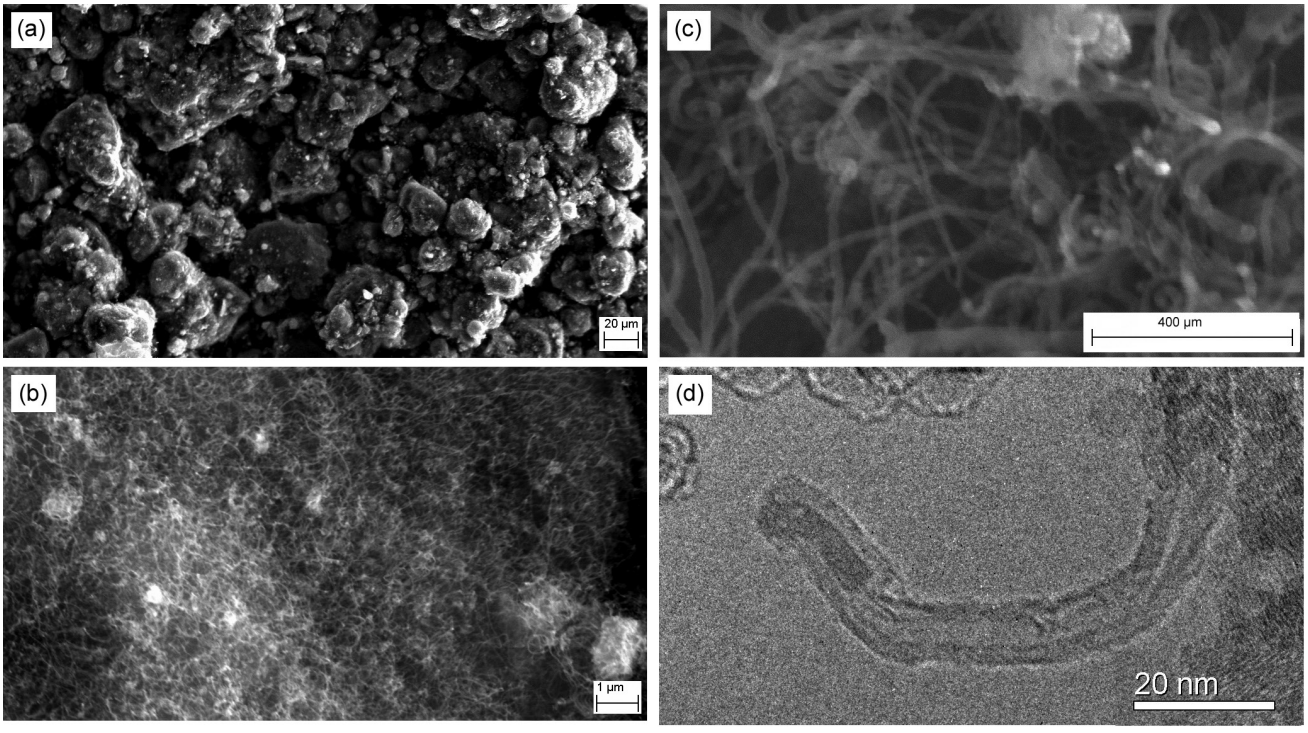

Figure 7. Images of carbon nanotubes prepared on 4Co/Al_2O_3 catalysts. (a), (b) and (c) SEM images at different magnifications; (d) TEM image.

the metallic surface area. The $4Co/Al_2O_3$ catalyst showed the highest production, 37.5%.

Combining the data obtained from TPO, Raman and electron microscopy, it was possible to estimate the amount of each carbon species produced in the reaction step. Three main different species can be produced in the carbon nanotube reaction step. These different carbon species oxidize at different temperatures. The TPO profiles of the carbon species present on the catalysts are illustrated in Figure 8. The 2 and $3Co/Al_2O_3$ catalysts showed low selectivity toward carbon nanotubes. In their profiles, there is a large peak at 380 °C related to amorphous carbon oxidation. These catalysts have shown metallic particle agglomeration in the reduction pretreatment. These agglomerated particles may not have the adequate shape or size for carbon nanotube growth. Table 5 shows the catalyst activity and selectivity of catalysts.

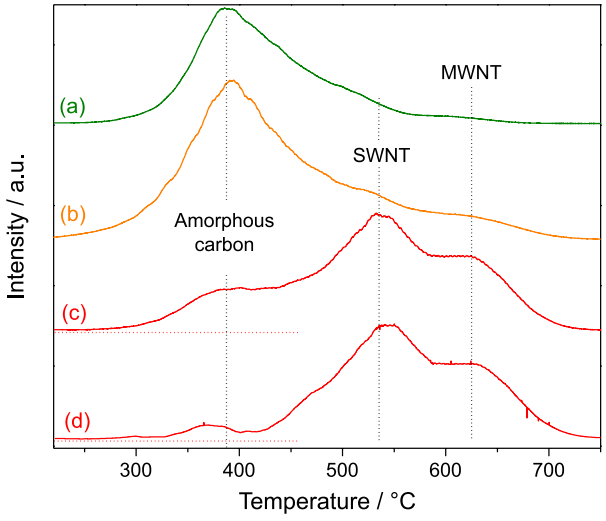

Figure 8. TPO profiles of the carbon species present on (a) $2Co/Al_2O_3$; (b) $3Co/Al_2O_3$; and (c) $4Co/Al_2O_3$. (d) TPO profiles of the carbon species present in $4Co/Al_2O_3$ after CNT reaction and oxidation step under 1% O_2/He (30 mL min^{-1}) at a heating rate of 2 °C min^{-1} up to 350 °C.

Raman

Raman spectroscopy provides information about the structure of carbon nanotubes and other carbon species. The tangential mode, called G band, at 1590 cm^{-1} is used to identify the presence of ordered carbon-like graphite and carbon nanotubes. The D band at 1350 cm^{-1} is related to defects on the carbon nanotube structure and the presence of amorphous carbon.[26-28] The intensity of the D band relative to the G band has been used as qualitative measurement of the formation of undesirable forms of carbon on nanotube production. Figure 9 shows the Raman spectra of carbon deposits formed on the catalysts.

The carbon deposits on the 2 and 3 Co/Al_2O_3 catalysts showed high D/G intensity ratios. These results indicate

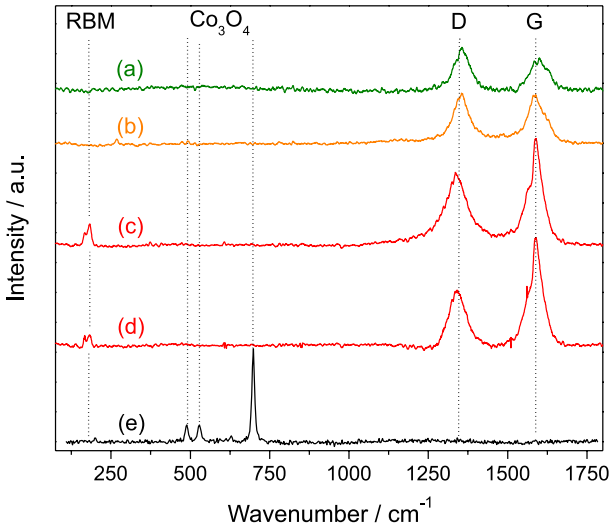

Figure 9. Raman spectra of the carbon deposits on (a) $2Co/Al_2O_3$; (b) $3Co/Al_2O_3$ and (c) $4Co/Al_2O_3$. (d) Spectrum of the carbon deposits on $4Co/Al_2O_3$ after CNT reaction and oxidation step under 1% O_2/He (30 mL min^{-1}) at a heating rate of 2 °C min^{-1} up to 350 °C. (e) Spectrum of the $4Co/Al_2O_3$ catalyst. RBM: radial breathing mode.

the presence of amorphous carbon and/or poorly structured carbon nanotubes, which were not observed on the SEM images. The TPO profile of these samples showed that most of the carbon deposits were amorphous carbon.

The D/G intensity ratio of carbon deposits on $4Co/Al_2O_3$ was lower than on the 2 and $3Co/Al_2O_3$ catalysts. The TPO profile also showed a decrease in the amorphous carbon fraction.

The influence of amorphous carbon in the Raman spectrum was verified by its oxidation for the $4Co/Al_2O_3$ catalyst. The oxidation consisted of a flow of 1% O_2/He (30 mL min^{-1}) at a heating rate of 2 °C min^{-1} up to 350 °C. Then, the sample was cooled under He flow until room temperature and a new TPO profile and a Raman spectrum were acquired, Figure 8d and Figure 9d, respectively. The new TPO profile showed a smaller fraction of amorphous carbon and the remnant carbon species deposited on the catalysts did not change their oxidation profile significantly. In the case of the Raman experiments, the D/G intensity improved to 0.5, indicating the amorphous carbon was removed by the oxidation at 350 °C.

The carbon deposits on the $4Co/Al_2O_3$ catalyst showed two small peaks at 167 and 183 cm^{-1}. These peaks are associated with single-walled carbon nanotubes (SWNT) and they are called radial breathing mode (RBM) peaks. TPO showed that 29% of carbon deposits on 4 Co/Al_2O_3 were SWNT. Some oxide species, like CoO, Co_3O_4 and $CoAl_2O_4$ can also show Raman peaks in the RBM region. In order to identify the cobalt oxide peaks, a Raman spectrum of the $4Co/Al_2O_3$ oxide catalyst was acquired, Figure 9e. There was not any overlap between the RBM peaks and

the cobalt oxide peaks. So, the peaks found at 167 and 183 cm^{-1} on spectra c and d in Figure 9 are from SWNT.

Conclusions

There are three main cobalt species in Co/γ-Al_2O_3 catalysts, $CoAl_2O_4$, CoO and Co_3O_4. Most cobalt in the 1Co/Al_2O_3 catalyst was present as $CoAl_2O_4$. This species was irreducible and highly dispersed on the support. Increasing the cobalt content of the catalysts led to a higher formation of Co_3O_4 as compared to the reducible CoO and $CoAl_2O_4$ species.

Catalysts with 2 and 3 wt.% of cobalt have cobalt oxide particles that reduced at low temperatures, lower than 400 °C. These particles agglomerated during the pretreatment step. These particles may not have the shape or size for carbon nanotube production.

The 4Co/Al_2O_3 catalyst showed high selectivity toward carbon nanotube production, mainly MWNT. The average metallic particle size is approximately the size of the carbon nanotube diameter, with the same correlation found in the literature.

Acknowledgments

We would like to thank Coordenação de Aperfeiçoamento de Pessoal de Nível Superior (CAPES) and Fundação de Amparo à Pesquisa do Estado do Rio de Janeiro (FAPERJ Proc. E-26/110.128/2013) for financial support and also Instituto Militar de Engenharia (IME) for the SEM images. We dedicate this manuscript to the memory of Prof Roberto Fernando de Souza, who acted for the development of the catalytic community in Brazil.

References

1. Cheng, H. M.; Li, F.; Su, G.; Pan, H. Y.; He, L. L.; Sun, X.; Dresselhaus, M. S.; *Appl. Phys. Lett.* **1998**, *72*, 3282.
2. Zhou, W. Y.; Bai, X. D.; Wang, E. G.; Xie, S. S.; *Adv. Mater.* **2009**, *21*, 4565.
3. Herrera, J. E.; Balzano, L.; Borgna, A.; Alvarez, W. E.; Resasco, D. E.; *J. Catal*. **2001**, *204*, 129.
4. Irurzun, V. M.; Tan, Y. Q.; Resasco, D. E.; *Chem. Mater*. **2009**, *21*, 2238.
5. Wen, Q.; Zhang, R. F.; Qian, W. Z.; Wang, Y. R.; Tan, P. H.; Nie, J. Q.; Wei, F.; *Chem. Mater*. **2010**, *22*, 1294.
6. Oliveira, H. A.; Franceschini, D. F.; Passos, F. B.; *J. Braz. Chem. Soc*. **2012**, *23*, 868.
7. Zowtiak, J. M.; Bartholomew, C. H.; *J. Catal*. **1983**, *83*, 107.
8. Reuel, R. C.; Bartholomew, C. H.; *J. Catal.* **1984**, *85*, 63.
9. Rane, S.; Borg, O.; Yang, J.; Rytter, E.; Holmen, A.; *Appl. Catal., A* **2010**, *388*, 160.
10. Sexton, B. A.; Hughes, A. E.; Turney, T. W.; *J. Catal.* **1986**, *97*, 390.
11. Carta, G.; Casarin, M.; El Habra, N.; Natali, M.; Rossetto, G.; Sada, C.; Tondello, E.; Zanella, P.; *Electrochim. Acta* **2005**, *50*, 4592.
12. Hilmen, A. M.; Schanke, D.; Hanssen, K. F.; Holmen, A.; *Appl. Catal., A* **1999**, *186*, 169.
13. Lee, J. C.; Kang, H. J.; Kim, K. J.; Kim, Y. S.; Moon, D. W.; *Surf. Sci.* **1976**, *324*, 338.
14. Kerkhof, F. P. J.; Moulijn, J. A.; *J. Phys. Chem.* **1979**, *83*, 1612.
15. Penn, D. R.; *J. Electron Spectrosc. Relat. Phenom.* **1976**, *9*, 294.
16. Liotta, L. F.; Pantaleo, G.; Macaluso, A.; Di Carlo, G.; Deganello, G.; *Appl. Catal., A* **2003**, *245*, 167.
17. Jongsomjit, B.; Panpranot, J.; Goodwin, J. G.; *J. Catal*. **2001**, *204*, 98.
18. Van Steen, E.; Sewell, G. S.; Makhothe, R. A.; Micklethwaite, C.; Manstein, H.; De Lange, M.; O'Connor, C. T.; *J. Catal*. **1996**, *162*, 220.
19. Storsaeter, S.; Totdal, B.; Walmsley, J. C.; Tanem, B. S.; Holmen, A.; *J. Catal*. **2005**, *236*, 139.
20. Zhang, J. L.; Chen, J. G.; Ren, J.; Sun, Y. H.; *Appl. Catal., A* **2003**, *243*, 121.
21. Chin, R. L.; Hercules, D. M.; *J. Phys. Chem.* **1982**, *86*, 360.
22. Nagaraju, N.; Fonseca, A.; Konya, Z.; Nagy, J. B.; *J. Mol. Catal. A: Chem.* **2002**, *181*, 57.
23. Chai, S. P.; Zein, S. H. S.; Mohamed, A. R.; *Chem. Phys. Lett*. **2006**, *426*, 345.
24. Dai, H.; *Surf. Sci*. **2002**, *500*, 218.
25. Stranick, M. A.; Houalla, M.; Hercules, D. M.; *J. Catal*. **1987**, *103*, 151.
26. Grimm, D.; Gruneis, A.; Kramberger, C.; *Chem. Phys. Lett.* **2006**, *428*, 416.
27. Saito, R.; Fujita, M.; Dresselhaus, G.; Dresselhaus, M. S.; *Appl. Phys. Lett*. **1992**, *60*, 2204.
28. Alvarez, W. E.; Pompeo, F.; Herrera, J. E.; Balzano, L.; Resasco, D. E.; *Chem. Mater*. **2002**, *14*, 1853.

Submitted: August 5, 2014
Published online: October 17, 2014